

Surface order-disorder phase transitions and percolation

M.C. Giménez, F. Nieto and A. J. Ramirez-Pastor[†]

Departamento de Física, Universidad Nacional de San Luis, CONICET,

Chacabuco 917, D5700BWS, San Luis, Argentina

cecigime@unsl.edu.ar; fnieto@unsl.edu.ar; antorami@unsl.edu.ar

Abstract

In the present paper, the connection between surface order-disorder phase transitions and the percolating properties of the adsorbed phase has been studied. For this purpose, four lattice-gas models in presence of repulsive interactions have been considered. Namely, monomers on honeycomb, square and triangular lattices, and dimers (particles occupying two adjacent adsorption sites) on square substrates. By using Monte Carlo simulation and finite-size scaling analysis, we obtain the percolation threshold θ_c of the adlayer, which presents an interesting dependence with $w/k_B T$ (being w , k_B and T , the lateral interaction energy, the Boltzmann's constant and temperature, respectively). For each geometry and adsorbate size, a phase diagram separating a percolating and a non-percolating region is determined.

Keywords: Percolation; Lattice-gas; Phase transitions; Monte Carlo simulation

PACS Numbers: 05.10.Ln; 64.60.Ak; 68.35.Rh; 68.35.Fx.

[†] To whom all correspondence should be addressed.

I. INTRODUCTION

Despite over three decades of intensive work, the interplay between percolation properties and thermal phase transitions is still an open problem. In this sense, the study of geometrical structures close to the critical point allows a better understanding of the mechanism of the phase transition^{1,2,3}. The geometric critical phenomena exemplified by percolation possess many striking parallels with the thermally driven critical phenomena, as it is provided by the Fortuin-Kasteleyn mapping⁴. Cluster description of thermodynamic phase transitions have been used since long time to elucidate the nature of the transitions by providing a geometrical interpretation of density correlations⁷. Fisher has introduced the phenomenological droplet model in which the fluctuations are associated to clusters or droplets which percolate at critical point⁸. More recently, it was concluded that the percolation transition can be considered as a particular case of the q -state Potts model where q is equal to 1^{5,6}, and can be described as a second order one, whose universality class depends only upon the space dimensionality. By following this line of reasoning, a wide variety of systems have been studied. Among the more recent contributions, the behavior of colloids and gels has been discussed in an interesting paper by A. Coniglio¹. The author concluded that it is very important to define the appropriate cluster for each phenomenon. Later, an important contribution has been made by S. Fortunato^{9,10} who analyzes the critical exponents of both the thermal and percolation phase transitions occurring for different models in two dimensions.

Although most of the works on the subject are devoted to the study of lattice-gas models in presence of attractive lateral interactions (or ferromagnetic coupling in magnetic language), there have been a few studies related to repulsive interactions and order-disorder phase transitions. In the last case, the definitions of connectivity and cluster of particles belonging to the adsorbed phase are not the same and the relationship between percolating clusters and critical points is non-trivial. In a previous paper¹¹, we studied the percolation of monomers on a square lattice as the particles interact with repulsive energies. The present contribution goes a step further, including honeycomb and triangular substrates and multisite-occupancy^{12,13,14,15,16} (adsorbates occupying more than one site).

The outline of the paper is as follows: In Section II we describe the lattice-gas model and the finite-size scaling theory. In Section III we present and discuss the results along

with general conclusions.

II. MODEL AND FINITE-SIZE SCALING THEORY

In order to consolidate the ideas involved here, four different physical systems have been considered, according to the adsorbate's size and surface geometry:

Model I): Monomers adsorbed on square lattices.

Model II): Monomers adsorbed on honeycomb lattices.

Model III): Monomers adsorbed on triangular lattices.

Model IV): Dimers adsorbed on square lattices.

In all cases, the substrate is represented by $M = L \times L$ equivalent adsorption sites with periodic boundary conditions.

To describe the system of N particles adsorbed on M sites at a given temperature T , let us introduce the occupation variable c_i which can take the following values: $c_i = 0$ if the corresponding site is empty and $c_i = 1$ if the site is occupied by an adatom (or dimer unit). Under these considerations, the Hamiltonian of the system is given by,

$$H = w \sum_{\langle i,j \rangle} c_i c_j - N(k-1)w + \epsilon_o \sum_i^M c_i \quad (1)$$

where w is the nearest-neighbor (NN) interaction energy (we focus on the case of repulsive lateral interactions among adsorbed particles, $w > 0$); $\langle i, j \rangle$ represents pairs of NN sites and $k = 1(2)$ for monomers(dimers). The term $N(k-1)w$ is subtracted in eq. (1) since, in the case of $k = 2$, the summation over all the pairs of NN sites overestimates the total energy by including N bonds belonging to the N adsorbed dimers. Finally, ϵ_o is the adsorption energy of the sites on the surface (we have taken $\epsilon_o = 0$ without loss of generality).

For fixed values of surface coverage, $\theta = kN/M$, and temperature T , the thermodynamic equilibrium is reached in the canonical ensemble by using a standard Kawasaki algorithm^{11,17}. Thus, a set of $m = 2000$ samples in thermal equilibrium is generated by taking configurations separated from each other by 1000 Monte Carlo steps in order to avoid memory effects.

The central idea of the percolation theory is based on finding the minimum concentration θ for which at least a cluster [a group of occupied sites in such a way that each site has at least one occupied nearest-neighbor site] extends from one side to the opposite one of the

system. This particular value of the concentration rate is named *critical concentration* or *percolation threshold* and determines a phase transition in the system.

It is well known that it is a quite difficult matter to analytically determine the value of the percolation threshold for a given lattice^{18,19,20,21,22}. Thus, in most cases, percolation thresholds have to be estimated numerically by means of computer simulations.

As the scaling theory predicts²³, the larger the system size to study, the more accurate the values of the threshold obtained therefrom. Thus, the finite-size scaling theory give us the basis to achieve the percolation threshold and the critical exponents of a system with a reasonable accuracy. For this purpose, the probability $R = R_L^X(\theta)$ that a lattice composed of $L \times L$ elements (sites or bonds) percolates at concentration θ can be defined¹⁸. Here, the following definitions can be given according to the meaning of X : a) $R_L^{R(D)}(\theta)$ = the probability of finding a rightward (downward) percolating cluster; b) $R_L^I(\theta)$ = the probability that we find a cluster which percolates both in a rightward **and** in a downward direction; c) $R_L^U(\theta)$ = the probability of finding either a rightward **or** a downward percolating cluster and d) $R_L^A(\theta) \equiv \frac{1}{2} [R_L^R(\theta) + R_L^D(\theta)] \equiv \frac{1}{2} [R_L^I(\theta) + R_L^U(\theta)]$. Based on these definitions and using the methodology described in Refs. [11,24,25,26,27,28,29,30,31,32,33], the percolation thresholds were calculated by extensive use of finite size scaling techniques. The interested reader is urged to read the above cited articles for a more complete discussion of this issue.

III. PERCOLATION PHASE DIAGRAM: RESULTS AND CONCLUSIONS

By using the scheme discussed above, the critical curves, θ_c vs. K (being $K \equiv w/k_B T$), separating the percolating and non-percolating regions, were calculated.

In Fig. 1, the percolation phase diagram is shown for Model I. As $K = 0$ (non-interacting adsorbate), the adsorption-desorption process reproduces a random deposition, which is fully equivalent to random percolation. Consequently, the expected value of $\theta_c = 0.592$ is reached for $K = 0$. As K is increased, two well-differentiated regimes can be distinguished: *i*) from $K = 0$ up to $K \approx 1.76$ (being $K \approx 1.76$ the reduced critical temperature for the order-disorder phase transition occurring in the system), θ_c increases linearly with K ; and *ii*) for $K > 1.76$, θ_c remains constant as K is increased. This behavior can be explained from simple geometrical arguments. Namely, lateral repulsive couplings avoid the occupation of nearest-neighbors sites, and consequently, increase the percolation

threshold. In the limit case, once K_c is reached, the adlayer does not vary significantly as K is increased, and θ_c reaches its saturation value, being $\theta_c \approx 0.66$ for $K > 1.76$. It is worth to emphasize that the presence of strong lateral interactions (and consequently, the existence of a phase transition occurring in the system) yields an increase in the computational effort to get accuracy values of the percolation threshold.

It is important to bear in mind that the points in Fig. 1 correspond to states in thermal equilibrium. In order to reflect this situation, we have calculated the adsorption isotherms (mean coverage as a function of the reduced chemical potential, $\mu/k_B T$) for repulsively interacting adparticles in a wide range of temperatures. The adsorption process was simulated through a Grand Canonical Ensemble Monte Carlo (GCEMC) method. Relaxation toward equilibrium relied upon Glauber dynamics³⁴.

For a given value of temperature T and chemical potential μ , an initial configuration with N monomers (dimers) adsorbed at random positions on N ($2N$) sites is generated. Then an adsorption-desorption process is started, where a site (pair of nearest-neighbor sites) is chosen at random and an attempt is made to change its occupancy state with probability given by the Metropolis rule³⁵:

$$P = \min \left\{ 1, \exp \left(-\Delta\tilde{H}/k_B T \right) \right\} \quad (2)$$

where $\tilde{H} = \tilde{H}_f - \tilde{H}_i$ is the difference between the effective Hamiltonians of the final and initial states, being $\tilde{H} = H - \mu \sum c_i$. A Monte Carlo Step (MCS) is achieved when N sites (pair of sites) have been tested to change its occupancy state. The equilibrium state can be well reproduced after discarding the first $m' = 10^5 - 10^6$ MCS. Then, averages are taken over $m = 10^5 - 10^6$ successive configurations. In this framework, the mean coverage is obtained as:

$$\theta = \frac{1}{N} \sum_i^N \langle c_i \rangle \quad (3)$$

where the thermal average $\langle \dots \rangle$, means the time average over the Monte Carlo simulation run.

In order to compare our numerical results with a theoretical prediction, we have used one of the most reliable methods for studying the thermodynamic properties of a system suffering a phase transition: the Real Space Renormalization Group (RSRG)³⁶. The interested reader is referred to Ref. [36,37] for a detailed description of the RSRG method and to Refs. [38,39,40,41] for applications of the RSRG method to lattice gas models.

In the RSRG method developed by Niemeyer and van Leeuwen⁴² and Nauenberg and Nienhuis^{43,44}, the whole lattice is divided into blocks (or cells) of L sites. A block spin S_α is assigned to each block. All blocks together must form a square lattice with the lattice constant $\sqrt{L}a$. The RSRG transformation of the spin system allows the reduction of the number of independent variables, i.e. the transition from the set of N site spins $\{s_i\}$ to N/L block spins $\{S_\alpha\}$. We note that two values of the block spin $S_\alpha = \pm 1$ corresponds to 2^L site spin configurations (since L spins are combined to form a block). For blocks with odd number of spins S_α is usually determined by the so-called “majority rule” (MR)³⁷. For even L a rule must be introduced in order to assign a definite value of the block spin to any given configuration with the sum of site spins equal to zero. In any case an obvious condition must be fulfilled: if the site spin configuration $\{s_1, s_2 \dots s_L\}$ is assigned to a block spin S_α with weighting factor P , then the configuration $\{-s_1, -s_2 \dots -s_L\}$ is assigned to the $-S_\alpha$ domain with the same P .

In the framework of the RSRG approach, one usually employs periodic boundary conditions. It is assumed that the whole lattice is given by the periodic continuation of a small cluster of blocks. In our calculations we consider the smallest possible cluster of two blocks. Due to the simplicity of this cluster, no additional interactions appear in the renormalized Hamiltonian. It is the same Hamiltonian of the square Ising spin system with, however, renormalized values for the external magnetic field and for the pair interaction parameter.

As was shown by Nauenberg and Nienhuis⁴³, the free energy of the system for any values of magnetic field and interaction parameter can be evaluated in a series of sequential RSRG transformations of the original Hamiltonian. The interested reader will find details of the application of this technique for Models I, II and III in the following references: square lattice, Ref. [45], triangular lattice, Ref. [46] and honeycomb lattice Ref. [47].

The results, obtained by Real Space Renormalization Group, RSRG (solid lines) and Monte Carlo, MC, methods (small squares), are shown in Fig. 2⁴⁵. At high temperatures the isotherms are close to the Langmuir case (lattice-gas without lateral interaction), i.e.

$$\theta(\mu) = \frac{\exp \beta(\mu + \varepsilon_o)}{1 + \exp \beta(\mu + \varepsilon_o)}. \quad (4)$$

At low temperatures a broad plateau occurs around half coverage. This plateau corresponds to the $c(2 \times 2)$ ordered lattice-gas phase (or, in magnetic language, to the AF ordered two-dimensional spin system). Large spheres in Fig. 2 are the same points as in

Fig. 1. It is clear that such line avoids to enter in the region of the coexistence of phases.

To reinforce the above result, in Fig. 3 the percolation line is plotted (spheres) together with the coexistence curve in the temperature-concentration diagram, which limits the region where the $c(2 \times 2)$ ordered phase percolates. As it can be observed, the percolation line remains in the region where the system is disordered. These features clearly reveal that the definitions of connectivity (in the sense of standard random percolation) and therefore the definitions of the clusters of $c(2 \times 2)$ ordered structure are not the same.

In the case of Model II (Fig. 4), the general trend is similar to that of the square lattice. The curve grows monotonically up to a value of $K \approx 2$, where it reaches an almost constant value of 0.75 for the critical coverage degree. The explanation of this trends is similar to the first case. The percolation line (spheres) plotted together with the adsorption isotherms for repulsively interacting particles adsorbed on a honeycomb lattice is shown in Fig. 5. In Fig. 6 the same line is plotted in conjunction with the phase diagram. Again, the percolation line remains in the region where the system is disordered.

For Model III (Fig. 7), it can be observed that the value of the percolation threshold is near 0.5 in the whole range of K (notice the scale in the graph). A complete understanding of the phase diagram is a very important help in the description of the peculiarities of the temperature dependence of the percolation threshold. In order to explain the antiferromagnetic ordering we recall that a triangular lattice can be seen as a system composed of three equivalent triangular sublattices. As is well known, pairwise interaction results in a symmetrical phase diagram around $\theta = 0.5$. For this lattice-gas system, triangular antiferromagnetic lattice-gas, the phase diagram (T, θ) consists of two symmetrical curves around $\theta = 0.5$. For $\theta \leq 1/3$, the ordered phase reveals that the particles are arranged in such a way that pairs of particles on nearest-neighbor lattice sites are not present. In fact, most of the adsorbed particles are located in only one of the three equivalent triangular sublattices, thus avoiding possible interactions with other particles (which is equivalent to an ordered $\uparrow\downarrow$ phase using magnetic language). This ordered phase prevails over the range $\theta \leq 0.5$ as is indicated in Fig. 8.

The symmetric branch of the phase diagram reflects the ordered phase where two of the sublattices are occupied ($\uparrow\downarrow$ in the magnetic language). This phase diagram has been investigated by Schick, Walker and Wortis^{48,49} by using RSRG as well as by the transfer matrix method⁵⁰ and MC simulations^{46,51}.

It is interesting to note that for $\theta \leq 0.5$ a) the corresponding ordered phase percolates but b) there is not standard percolation of the adsorbed monomers on the lattice. The percolation line dividing the percolating and non percolating area yields in the disordered phase of the antiferromagnetic phase diagram (see Fig. 8). Furthermore, in the whole range of temperature, the percolation occurs for a coverage lower than what is needed to build the ordered phase for $\theta \geq 0.5$

Fig. 9 shows the percolation line together with the adsorption isotherms for repulsively interacting particles. The adsorption isotherms present clearly defined plateaus located at $\theta = \frac{1}{3}$ and $\theta = \frac{2}{3}$. Strong enough repulsion produces ordered phases when particles occupy preferentially sites of a single sublattice ($\theta = \frac{1}{3}$), or two sublattices ($\theta = \frac{2}{3}$).

In the case of dimers on square lattices (Fig. 10), the curve θ_c vs. K (spheres) is similar to that of Fig. 1 (open circles). Thus, θ_c grows linearly from $\theta_c(K = 0) = 0.56$ (as it is expected for random percolation of dimers) to a saturation value close to $2/3$. This behavior has interesting consequences on the temperature-concentration phase diagram. In fact, as it has been reported in the literature¹³, a “zig-zag” (ZZ) ordered phase, characterized by domains of parallel ZZ strips oriented at $\pm 45^\circ$ from the lattice symmetry axes, separated from each other by strips of single empty sites, was found at $2/3$ monolayer coverage (Fig. 11). The ordered phase is separated from the disordered state by a order-disorder phase transition occurring at a finite critical temperature. An accurate determination of this critical temperature has been recently obtained [$k_B T_c/w = 0.182(1)$]⁵².

A simple inspection of Fig. 11 shows the existence of long-range connectivity for the low-temperature phase at $2/3$ coverage. This finding, along with the tendency to $2/3$ of the curve in Fig. 10, clearly reveals the interplay between the surface order-disorder phase transition and the percolating properties of the adsorbed phase at $2/3$ monolayer coverage. Namely, *i*) the ZZ ordered phase represents the state of the adlayer at percolation threshold and $K \rightarrow \infty$ and *ii*) the curve θ_c vs. K crosses the coexistence line on the temperature-concentration phase diagram at $(\theta_c = 2/3, k_B T_c/w = 0.181)$ and penetrates in the ZZ-region. The last point represents the main difference between Model IV and the other models previously analyzed. A systematic analysis of critical exponents was not carried out since this was out of the scope of the present work.

Since properties of adsorbed layers are often determined by measuring adatom coverage

versus adsorbate gas pressure, it is important to show what adsorption isotherms would look in this case. Thus, Fig. 12 shows a set of adsorption isotherms for dimers and different values of repulsive nearest-neighbor interactions together with the percolation line. Since the symmetry particle-vacancy, valid for monoatomic species, is broken for dimers, the adsorption isotherms are not symmetric around $\theta = 0.5$. In addition, two well defined and pronounced steps appears as K increases. At $\theta = 0.5$, a well defined array of dimers resembling a $c(2 \times 2)$ phase, is found. The ordered structure is characterized by a repetition of alternating files of adsorbed dimers separated by 2 adjacent empty sites. As the chemical potential μ increases and θ approaches $\theta = 2/3$, incoming dimers are adsorbed forming domains of parallel zig-zag rows (ZZ phase) as it was discussed above. These structures are clearly evidence of a low temperature ordered phase. In fact, the systems undergoes continuous phase transitions, from disorder to ordered structures^{15,16,52}.

In summary, we presented a model to investigate the process of adsorption of interacting monomers on square, honeycomb and triangular lattices and studied the percolating properties of the adsorbed phase. By using Monte Carlo simulation and finite-size scaling theory, we obtained the percolation thresholds for different values of concentration and temperature. From this analysis, a critical curve in the $\theta - T$ space was addressed. The line separating the percolating and non-percolating regions was explained in terms of simple considerations related to the interactions present in the problem.

Acknowledgements

This work was supported in part by CONICET (Argentina) and the Universidad Nacional de San Luis (Argentina) under projects PIP 6294 and 322000, respectively. The numerical work were done using the BACO parallel cluster (composed by 60 PCs each with a 3.0 MHz Pentium-4 processors) located at Laboratorio de Ciencias de Superficies y Medios Porosos, Universidad Nacional de San Luis, San Luis, Argentina.

Figure Captions

Fig. 1: Phase diagram, θ_c versus K , which shows the curve separating the percolating and nonpercolating regions for the case of monomers on a square lattice. The vertical dashed line at $K = 1.76$ denotes the reduced critical temperature for the phase transition occurring in the adlayer phase for repulsive interacting particles. Horizontal dashed line at $\theta_c = 0.662$ is the critical coverage at saturation regime for $K > 1.76$. The error bars are smaller than the symbol size.

Fig. 2: Adsorption isotherms for Model I (surface coverage, θ , vs. normalized chemical potential, $\mu/k_B T$ and reciprocal temperature expressed in units of K). Solid lines are obtained by the RSRG method, small symbols denote MC data while large spheres are the same points as in Fig. 1.

Fig. 3: Phase diagram (critical temperature versus surface coverage) corresponding to Model I obtained by RSRG, solid line. Phase diagram, K^{-1} versus θ_c , which shows the curve separating the percolating and nonpercolating regions, spheres. The inset is a snapshot of the ordered phase $c(2 \times 2)$.

Fig. 4: Phase diagram, θ_c versus K , for Model II. The critical coverage at saturation regime is $\theta_c = 0.758$. The error bars are smaller than the symbol size.

Fig. 5: Adsorption isotherms for Model II and different values of K , as indicated with small symbols. Solid lines are obtained by the RSRG method, small symbols denote MC data while large spheres are the same points as in Fig. 4.

Fig. 6: Phase diagram (critical temperature versus surface coverage) corresponding to Model II obtained by RSRG, solid line. Phase diagram, K^{-1} versus θ_c , which shows the curve separating the percolating and nonpercolating regions, spheres. The inset is a snapshot of the ordered phase.

Fig. 7: Phase diagram, θ_c versus K , for Model III. The error bars are included in the figure.

Fig. 8: Phase diagram (critical temperature versus surface coverage) corresponding to Model III obtained by RSRG, solid line. It consists of two symmetrical curves around $\theta = 0.5$. The first one, for $\theta < 0.5$ limits the ordered phase where the particles are arranged in such a way that pairs of particles on nearest-neighbor lattice sites are not present (which is equivalent to an ordered $\uparrow\downarrow$ phase using magnetic language). The

second one, reflects the ordered phase where two of the sublattices are occupied ($\uparrow\uparrow\downarrow$). The insets are snapshots of the corresponding ordered phases. Phase diagram, K^{-1} versus θ_c , which shows the curve separating the percolating and nonpercolating regions, spheres.

Fig. 9: Adsorption isotherms for Model III and different values of K , as indicated with small symbols. Solid lines are obtained by the RSRG method, small symbols denote MC data while large spheres are the same points as in Fig. 7.

Fig. 10: Phase diagram θ_c vs. K for Model IV (spheres) plotted together with data of Model I for comparison (open circles).

Fig. 11: Phase diagram (critical temperature versus surface coverage) corresponding to Model IV, solid line. It consists of curves representing the regions where the phases plotted in the insets are stables. Phase diagram, K^{-1} versus θ_c , which shows the curve separating the percolating and nonpercolating regions, spheres.

Fig. 12: Adsorption isotherms for Model IV and different values of K , as indicated. Small symbols denote MC data while large spheres are the same points as in Fig. 10.

-
- ¹ A. Coniglio, J. Phys.: Condens. Matter **13**, 9039 (2001).
- ² A. Coniglio, Nuclear Physics A **681**, 451 (2001).
- ³ A. Coniglio, Physica A **281**, 129 (2000).
- ⁴ C. M. Fortuin and P. W. Kasteleyn, Physica **57**, 536 (1972)
- ⁵ P. W. Kasteleyn and C. M. Fortuin, J. Phys. Soc. Japan Suppl. **16**, 11 (1969).
- ⁶ F. Y. Wu, Rev. Mod. Phys. **54**, 235 (1982).
- ⁷ T.L. Hill, *Statistical Mechanics* (New York, Mc Graw-Hill, 1956).
- ⁸ M.E. Fisher, Physics (N.Y.) **3**, 225 (1967) .
- ⁹ S. Fortunato, Phys. Rev. B **66**, 054107 (2002).
- ¹⁰ S. Fortunato, Phys. Rev. B **67**, 014102 (2003).
- ¹¹ M. C. Giménez, F. Nieto, A.J. Ramirez-Pastor, J. Phys. A: Math. Gen. **38**, (2005) 3253.
- ¹² W. Rudziński and D. H. Everett, *Adsorption of Gases on Heterogeneous Surfaces* (Academic Press, New York, 1992).
- ¹³ A. J. Ramirez-Pastor, J. L. Riccardo and V. Pereyra, Surf. Sci. **411**, 294 (1998).
- ¹⁴ A. J. Ramirez-Pastor, T. P. Eggarter, V. D. Pereyra and J. L. Riccardo, Phys. Rev. B **59**, 11027 (1999).
- ¹⁵ F. Romá, A. J. Ramirez-Pastor and J. L. Riccardo, Phys. Rev. B **68**, 205407 (2003).
- ¹⁶ F. Romá, A. J. Ramirez-Pastor and J. L. Riccardo, Phys. Rev. B **72**, 035444 (2005).
- ¹⁷ K. Kawasaki, in C. Domb and M. Green, editors, *Phase Transitions and Critical Phenomena*, Vol. 2, (Academic, London, 1972).
- ¹⁸ D. Stauffer, *Introduction to Percolation Theory*, (Taylor & Francis, London, 1985).
- ¹⁹ M. Sahimi, *Application of the percolation theory*, (Taylor & Francis, London, 1992).
- ²⁰ R.Zallen, *The Physics of Amorphous Solids*, (John Willey & Sons, NY, 1983).
- ²¹ J.W. Essam, Report on Progress in Physics **43**, 843 (1980).
- ²² J.-P. Hovi and A. Aharony, Phys. Rev. B **53**, 235 (1996).
- ²³ K. Binder, Reports on Progress in Physics **60**, 488 (1997).
- ²⁴ F. Yonezawa, S. Sakamoto and M. Hori, Phys. Rev. B **40**, 636, (1989).
- ²⁵ F. Yonezawa, S. Sakamoto, and M. Hori, Phys. Rev. B **40**, 650, (1989).
- ²⁶ V. Cornette, A.J. Ramirez-Pastor and F. Nieto, Physica A **327**, 71 (2003).
- ²⁷ V. Cornette, A.J. Ramirez-Pastor and F. Nieto, Eur. Phys. J. B **36**, 391 (2003).
- ²⁸ M. Dolz, F. Nieto, A.J. Ramirez-Pastor, Eur. Phys. J. B **43**, 363 (2005).
- ²⁹ M. Dolz, F. Nieto, A.J. Ramirez-Pastor, Phys. Rev. E **72**, 066129 (2005).
- ³⁰ G.M.T. Watts, J. Phys. A: Math. Gen. **29**, L363 (1996).
- ³¹ R. Langlands, P. Pouliot and Y. Saint-Aubin, Bull. Am. Math. Soc. **30**, 1 (1994).
- ³² R. Langlands, C. Pichet, P. Pouliot and Y. Saint-Aubin, J. Stat. Phys. **67**, 553 (1992).
- ³³ J.L. Cardy, J. Phys. A: Math. Gen. **25**, L201 (1992); Nucl. Phys. B **324**, 581 (1989); Nucl. Phys. B **275**, 200 (1986).
- ³⁴ D. Nicholson and N. G. Parsonage, *Computer Simulation and Statistical Mechanics of Adsorption*, (Academic Press, London, 1982).
- ³⁵ N. Metropolis, A. W. Rosenbluth, M. N. Rosenbluth, A. W. Teller, E. Teller, J. Chem. Phys. **21**, 1087 (1953).
- ³⁶ K.G. Wilson , Rev. Mod. Phys. **47** 773 (1975).

- ³⁷ Th. Niemeijer and J. M. J. van Leeuwen, *Renormalization Theory for Ising-like Spin Systems* in *Phase Transitions and Critical Phenomena*, edited by C. Domb and M. S. Green (Academic, New York, 1976), Vol.6, Chap.7.
- ³⁸ G. D. Mahan and F. H. Claro, Phys.Rev. B **16**, 1168 (1977).
- ³⁹ A.N. Berker, S. Ostlund, and F.A. Putnam, Phys. Rev. B **17**, 3650 (1978).
- ⁴⁰ R.G. Caflisch and A.N. Berker, Phys. Rev. B **29**, 1279 (1984).
- ⁴¹ R.G. Caflisch, A.N. Berker, and M. Kardar, Phys. Rev. B **31**, 4527 (1985).
- ⁴² Th. Niemeijer and J. M. J. van Leeuwen, Physica **71**, 17 (1974).
- ⁴³ M. Nauenberg and B. Nienhuis, Phys.Rev.Lett. **33**, 1598 (1974).
- ⁴⁴ B. Nienhuis and M. Nauenberg, Phys.Rev.Lett. **35**, 477 (1975).
- ⁴⁵ A.A. Tarasenko, L. Jastrabik, F. Nieto and C. Uebing, Phys. Rev. B **59**, 8252 (1999); Physical Chemistry Chemical Physics (PCCP) **1**, 1583 (1999); A.A. Tarasenko, F. Nieto, L. Jastrabik and C. Uebing. The European Physical Journal D **12**, 311 (2000).
- ⁴⁶ A.A. Tarasenko, F. Nieto and C. Uebing. Physical Chemistry Chemical Physics (PCCP), **2** 3453 (2000); A.A. Tarasenko, F. Nieto, L. Jastrabik and C. Uebing. Phys. Rev. B **64** 0754131 (2001); Surface Science **536**, 1 (2003) 1-14; F. Nieto, A.A. Tarasenko, "Collective surface diffusion of interacting particles on a triangular lattice: real-space renormalization group and Monte Carlo approaches" in "Trends in Surface Science Research", Editor: Charles P. Norris, Nova Science Publishers, Inc., New York, (2005).
- ⁴⁷ A. A. Tarasenko, L. Jastrabik and C. Uebing Phys. Rev. B **57**, 10166 (1998).
- ⁴⁸ M. Schick, J. S. Walker and M. Wortis, Phys.Lett. A **58**, 479 (1976).
- ⁴⁹ M. Schick, J. S. Walker and M. Wortis, Phys. Rev. B **16**, 2205 (1977).
- ⁵⁰ W. Kinzel and M. Schick, Phys. Rev. B **23**, 3435 (1981).
- ⁵¹ B.D. Metcalf, Phys. Lett. A **45**, 1 (1973).
- ⁵² F. Romá, J. L. Riccardo and A.J. Ramirez-Pastor, *Critical behavior of repulsive dimers at 2/3 monolayer coverage*, submitted (2006).

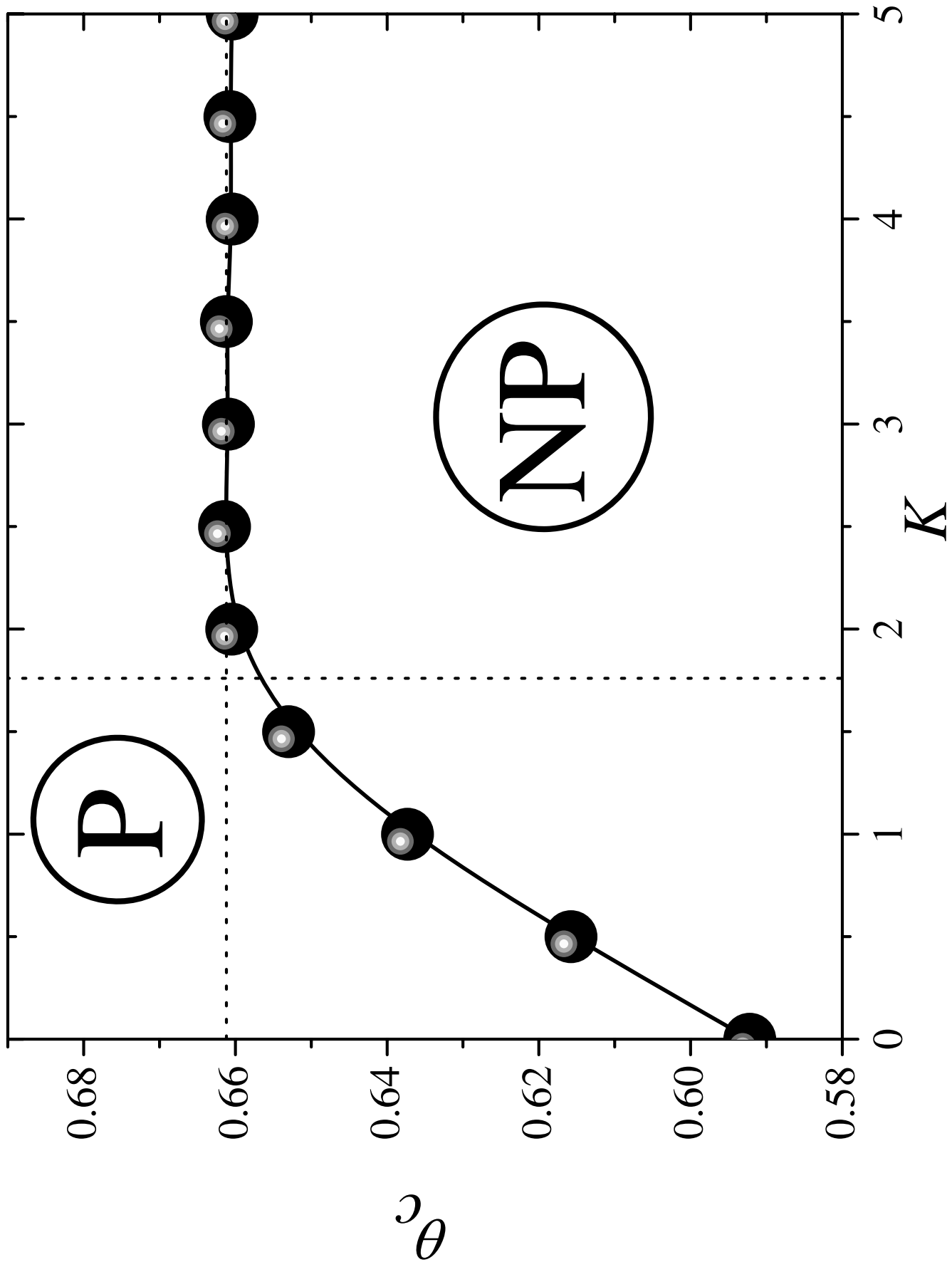


Fig.1

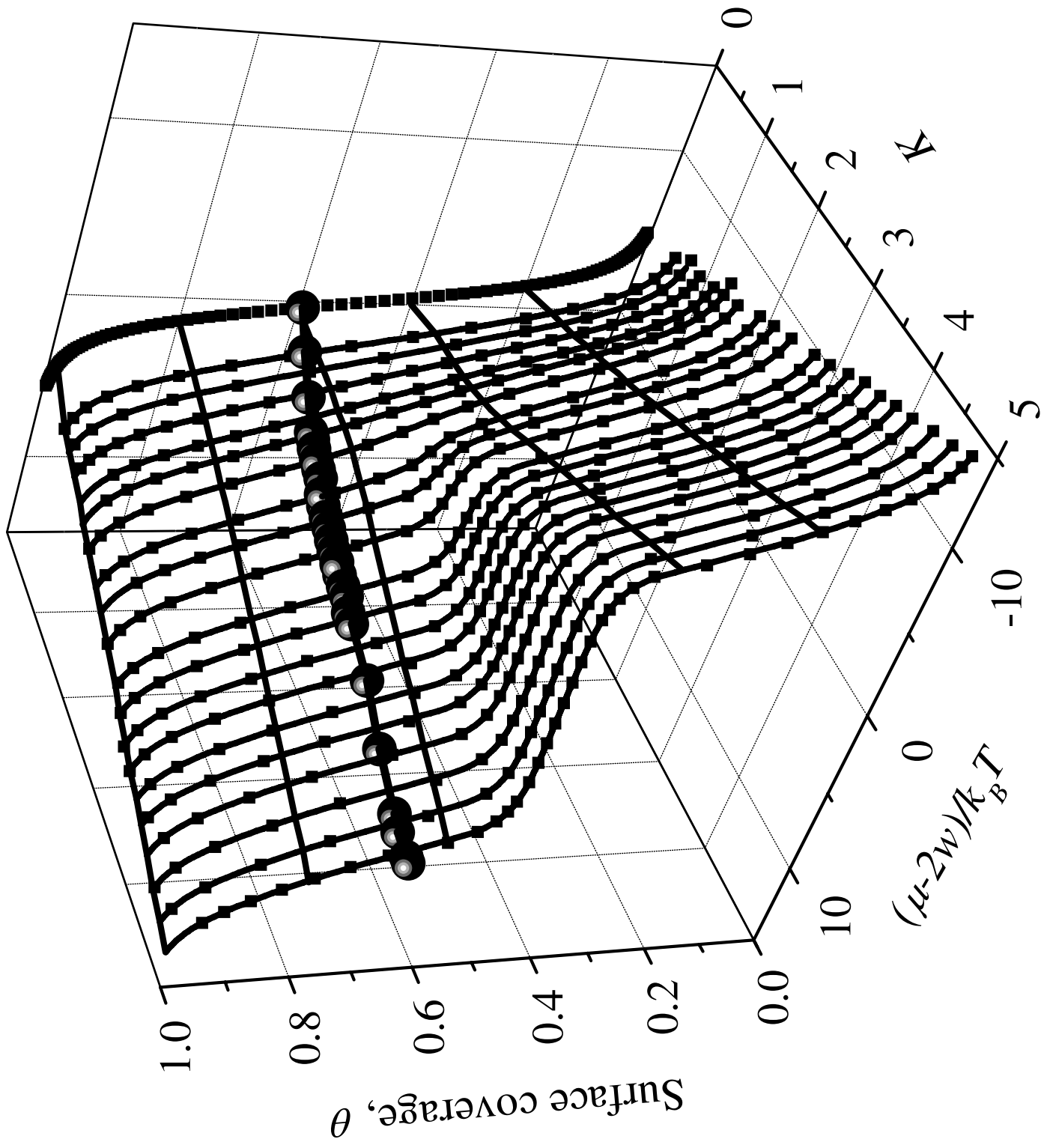
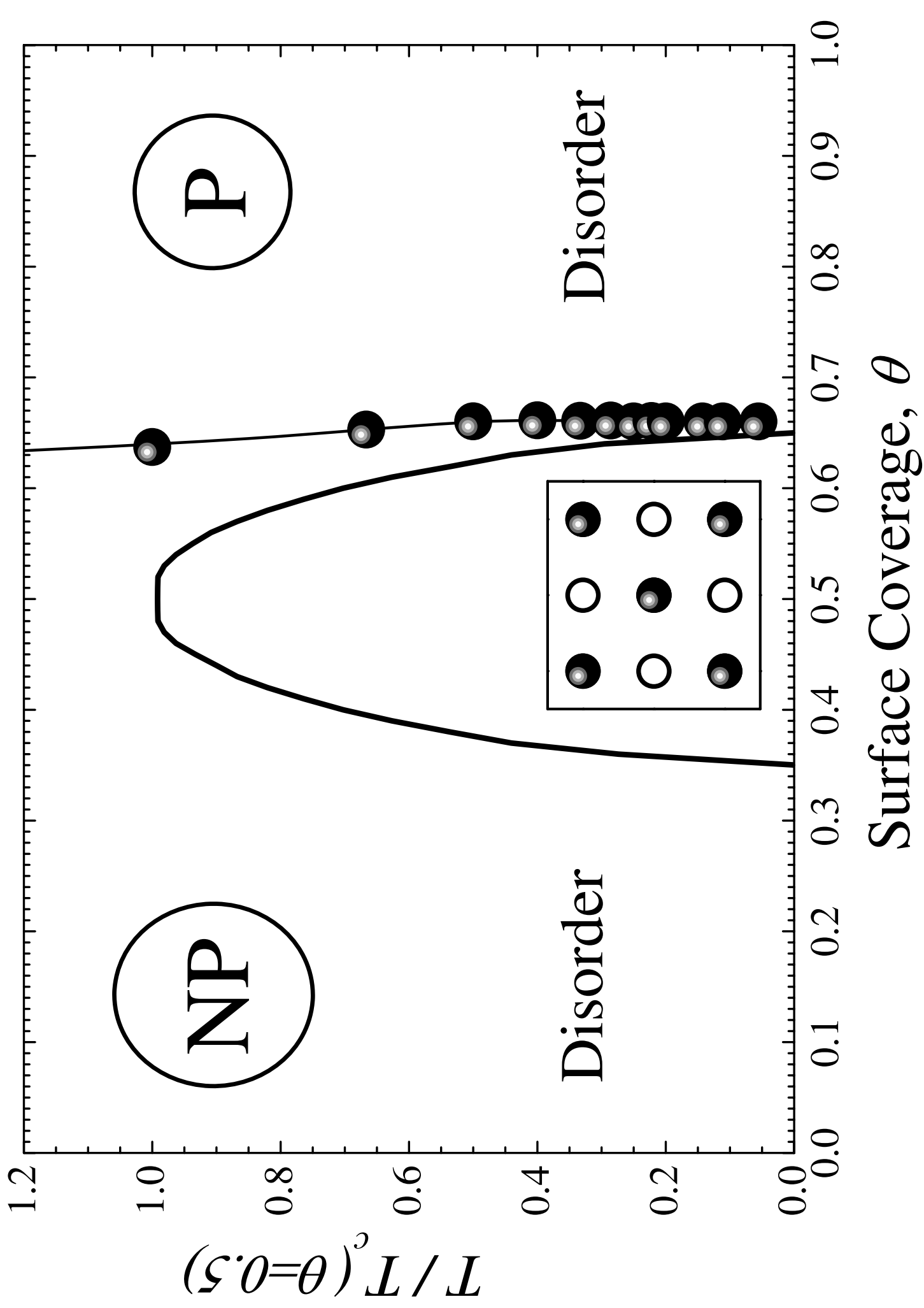
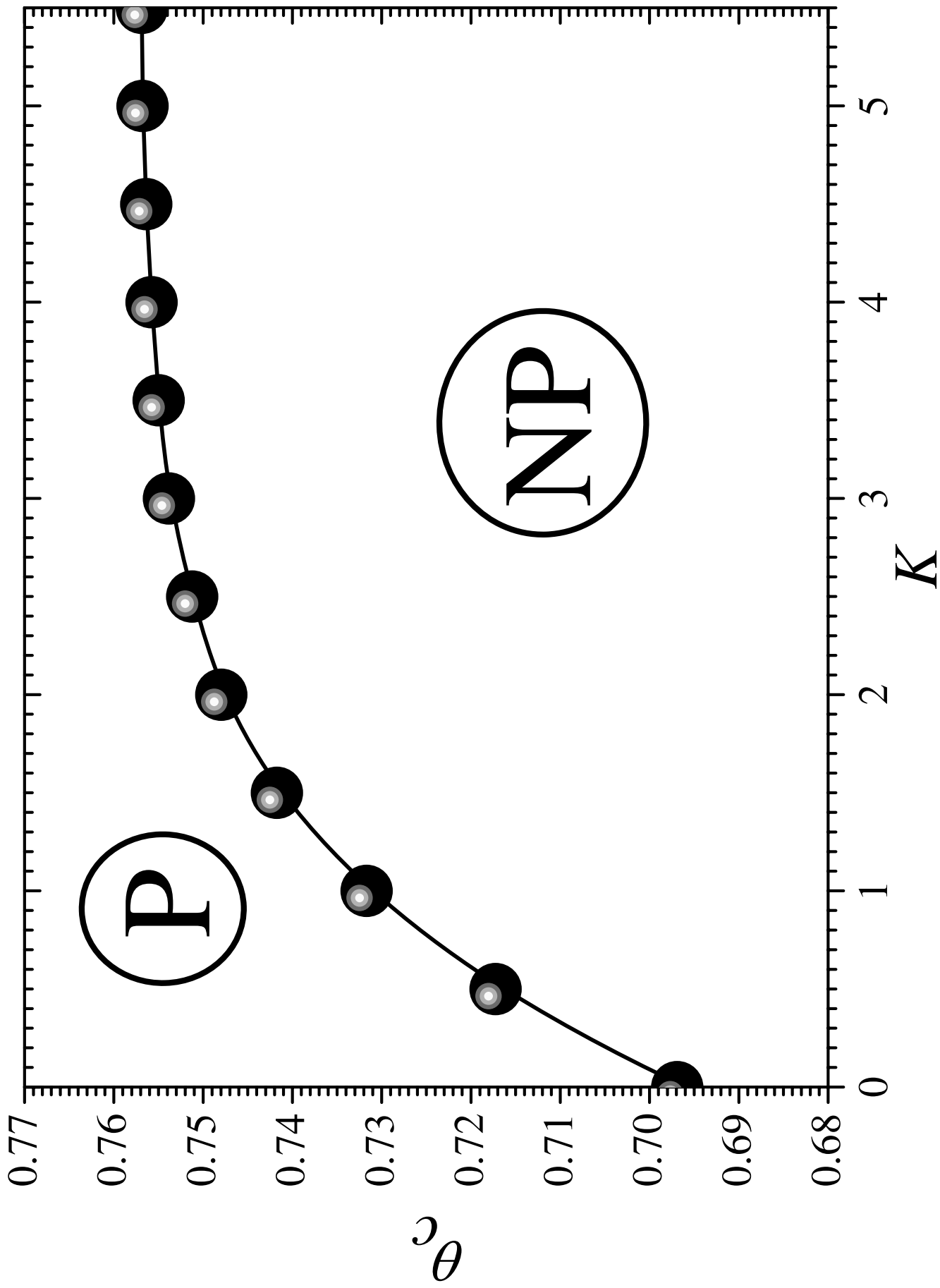
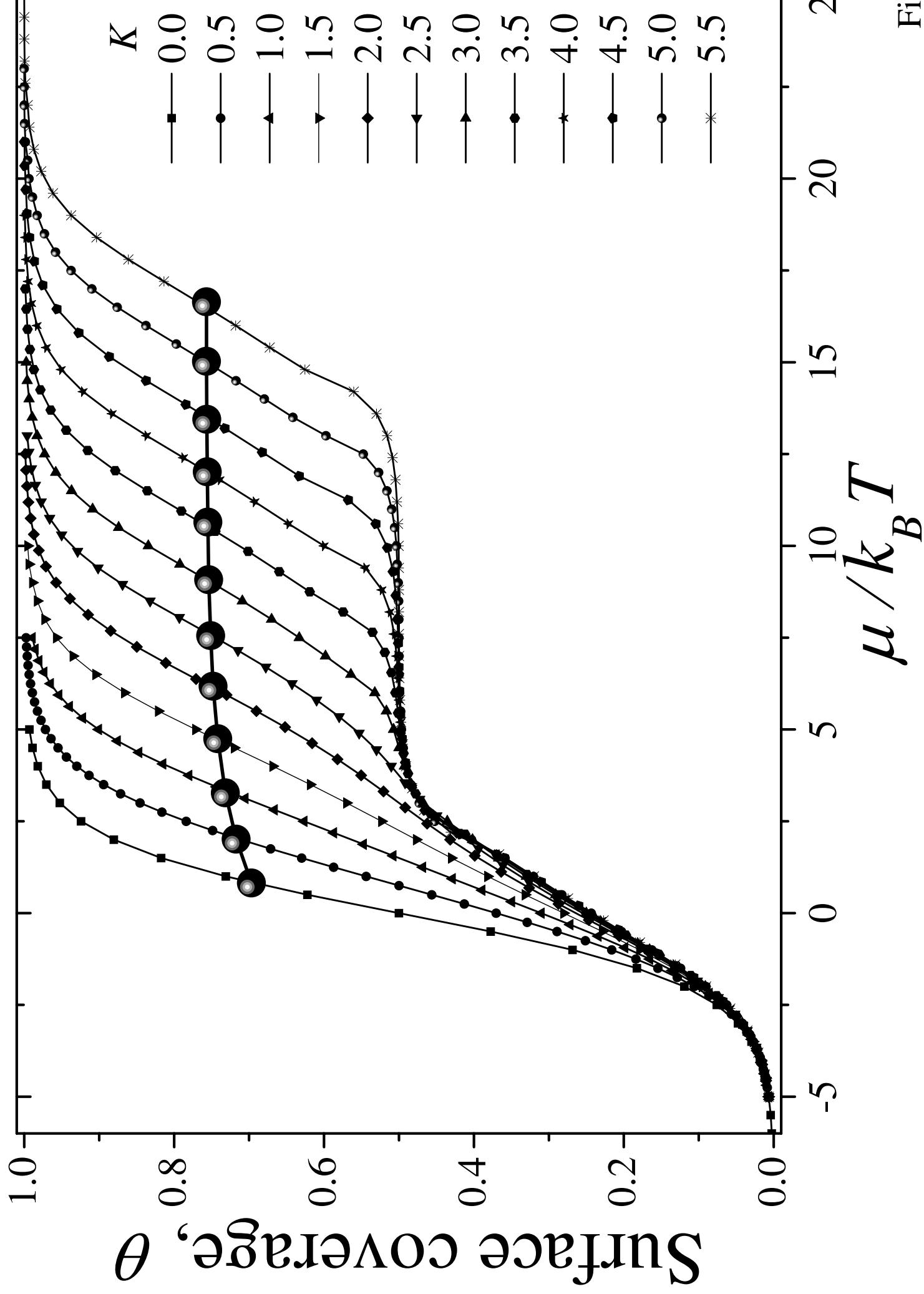


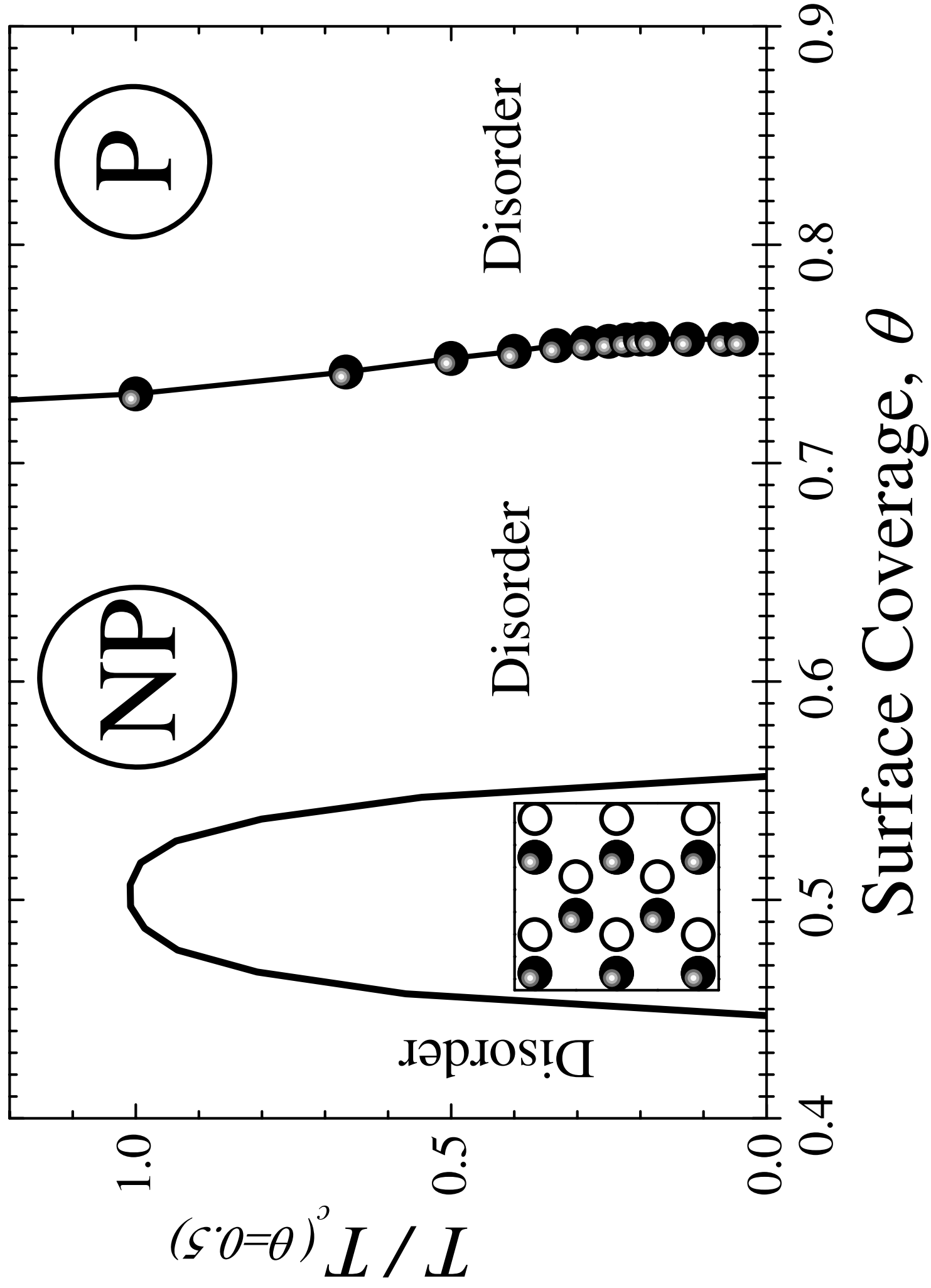
Fig. 2





Fig





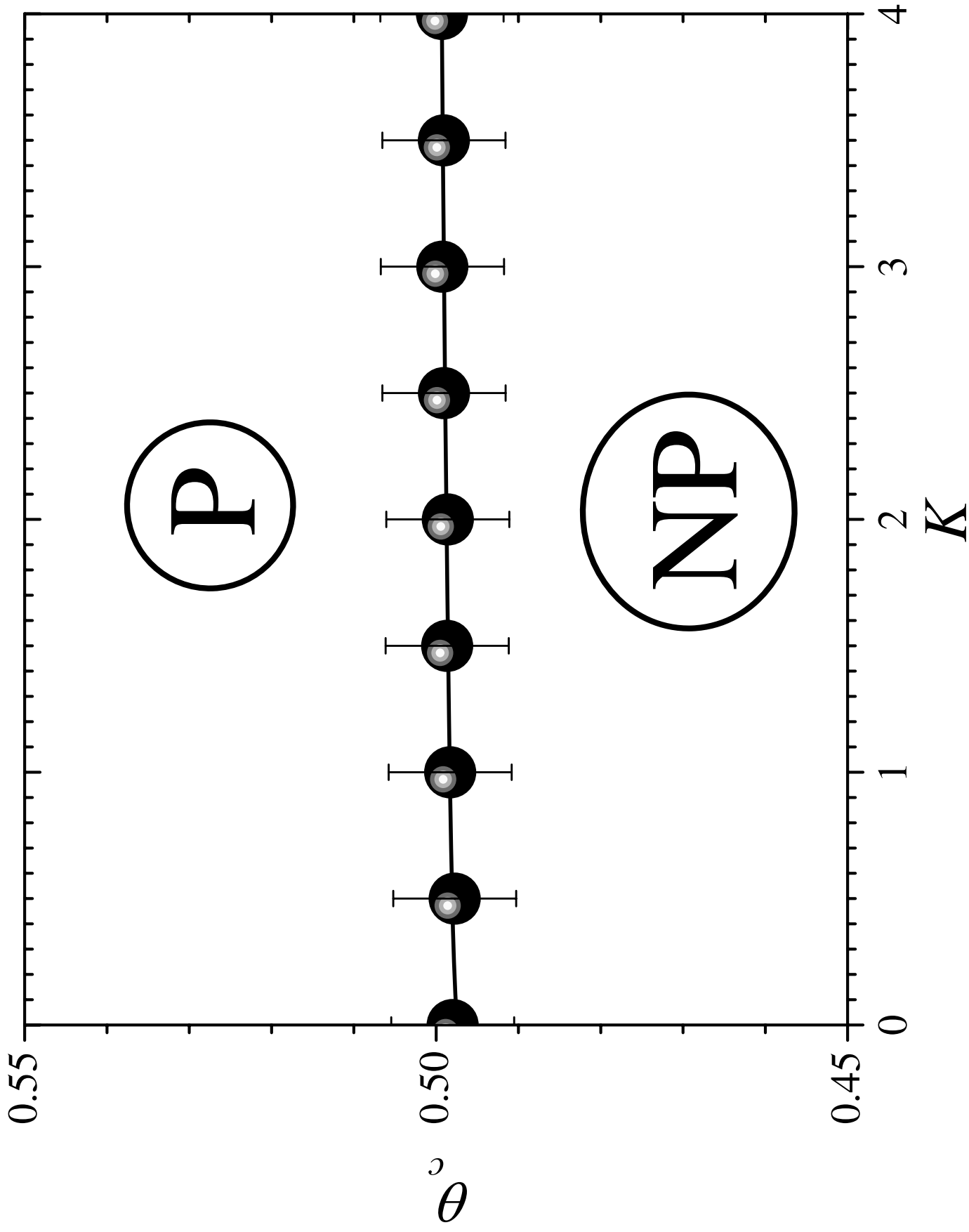
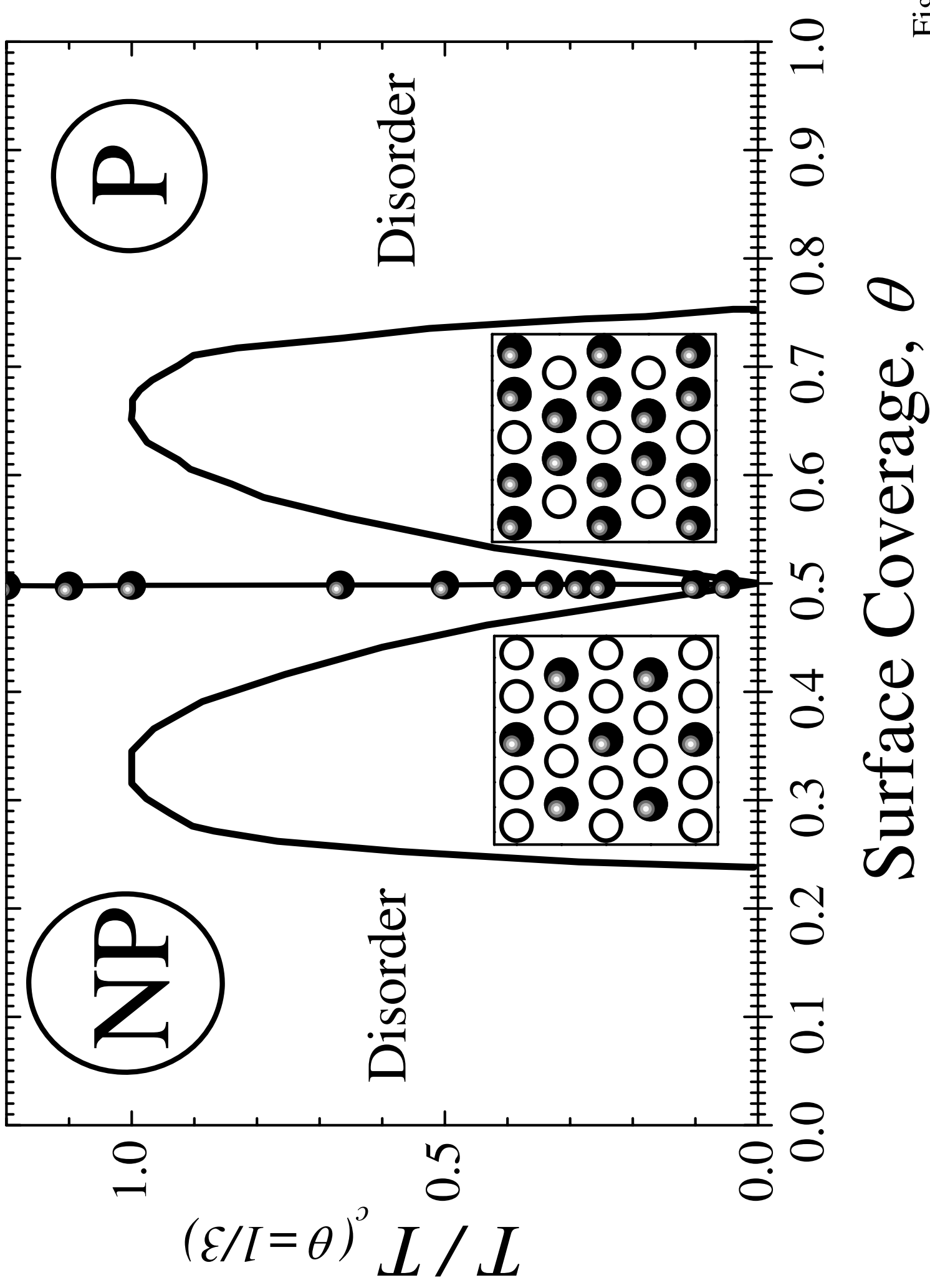
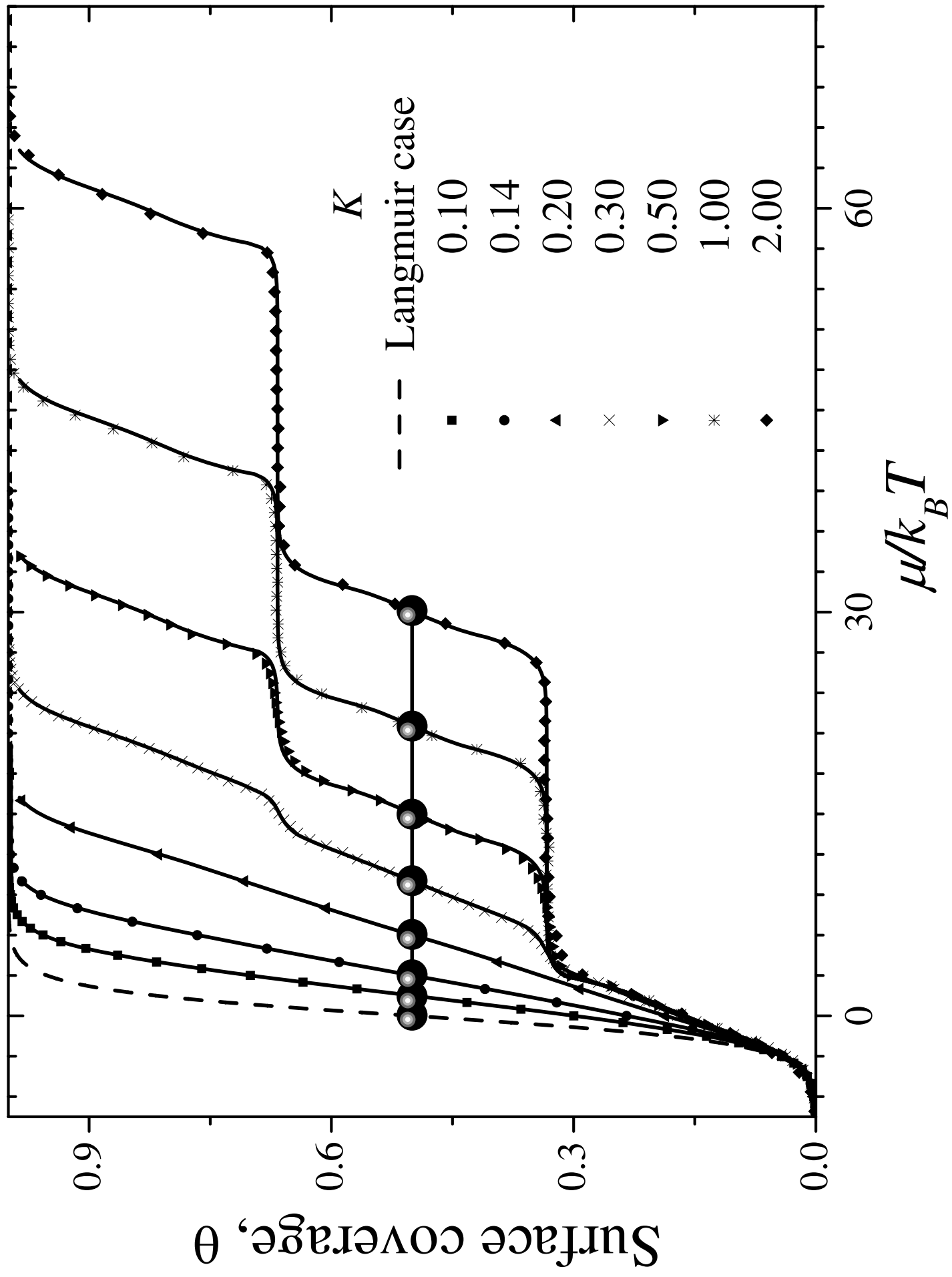
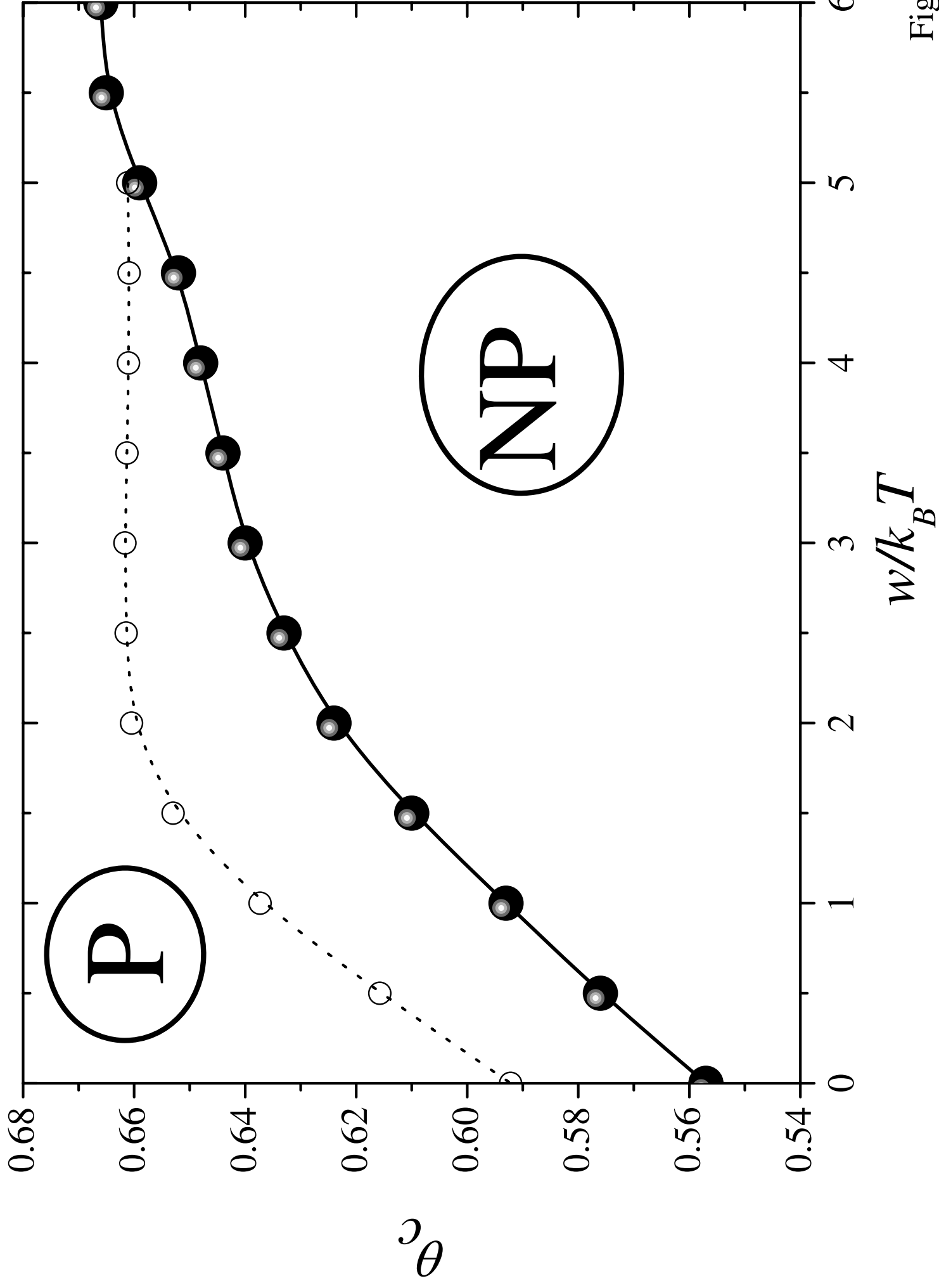


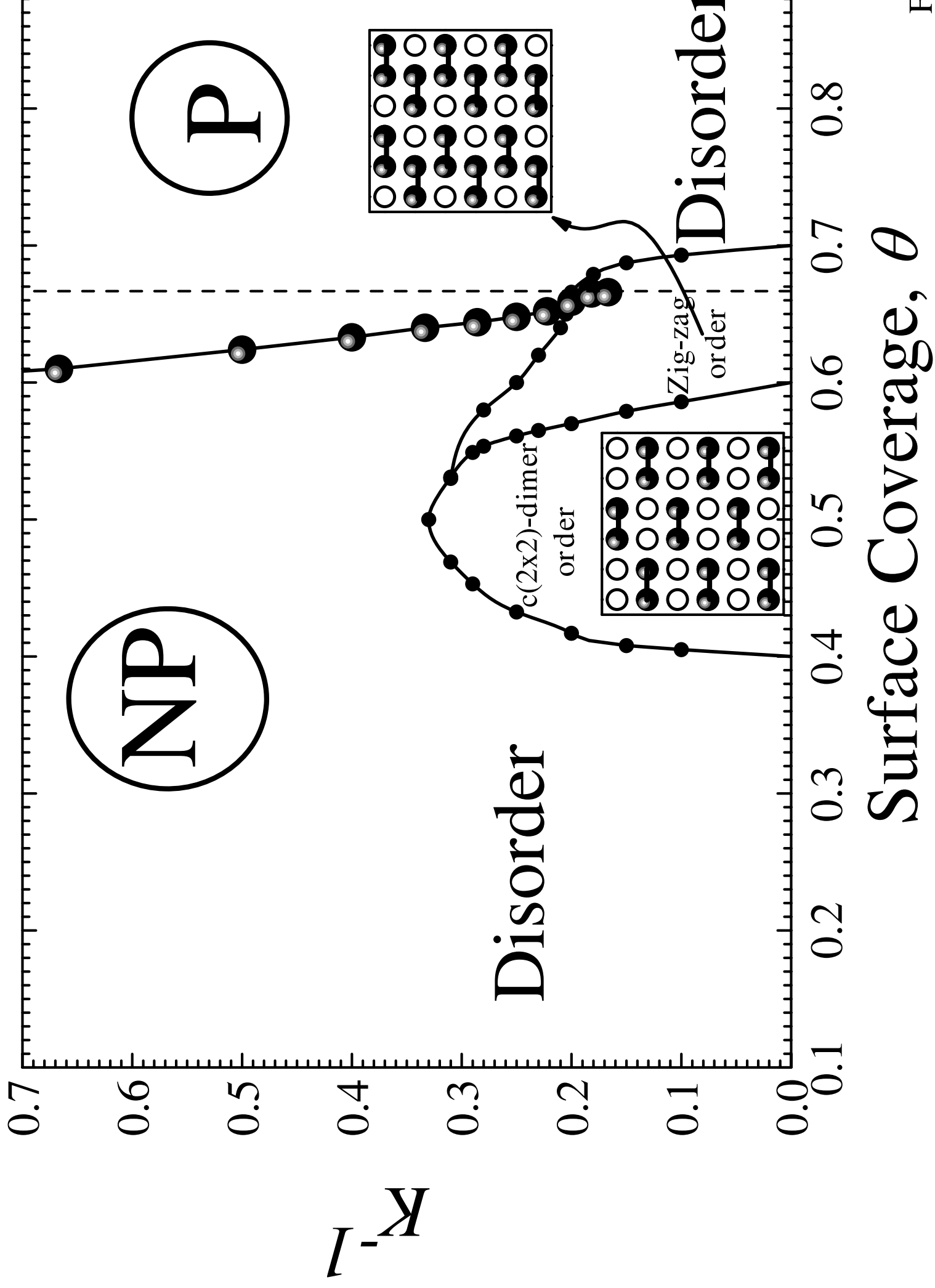
Fig.7







Fig



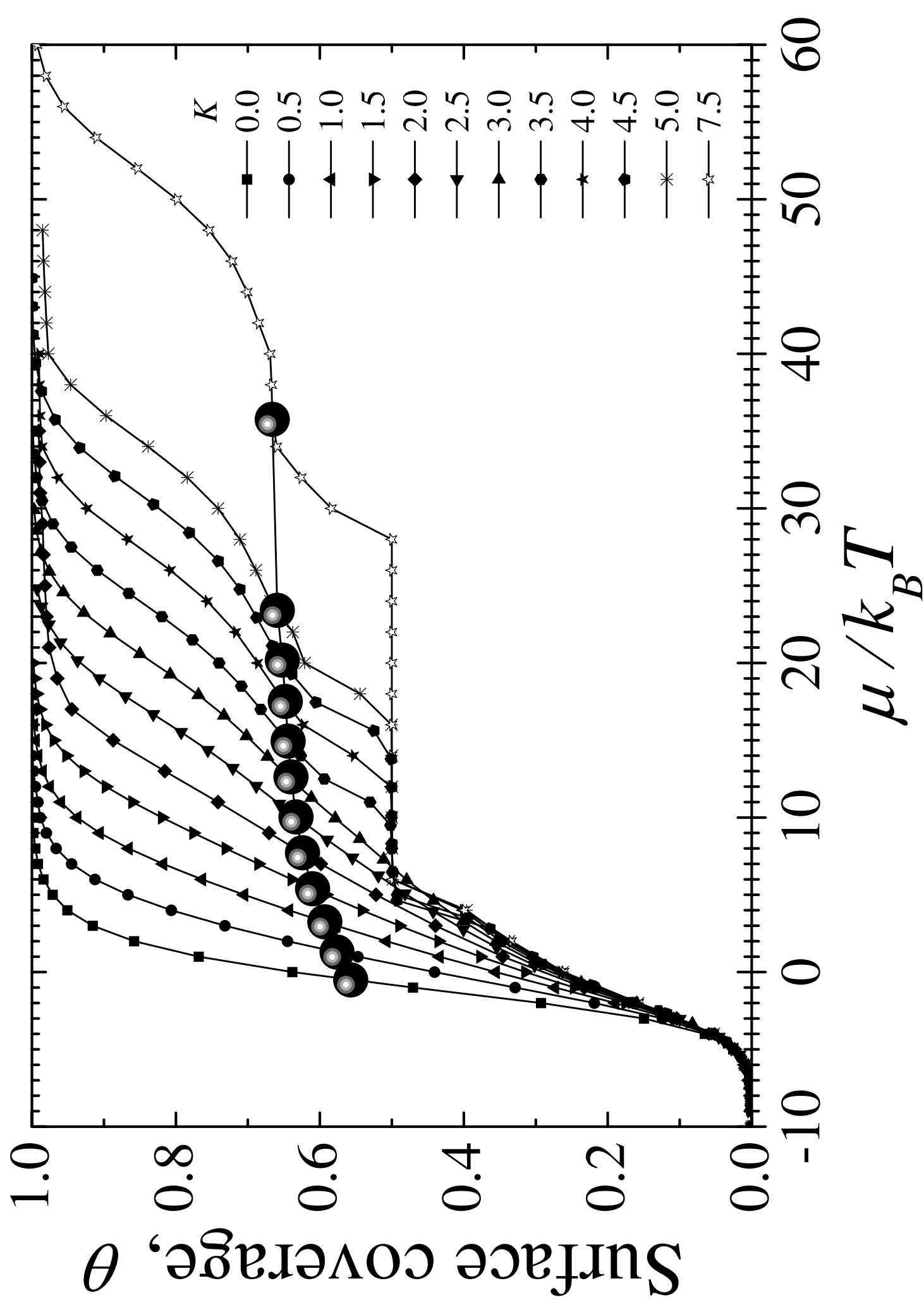


Fig. 12